J. Fluid Mech. (2017), *vol.* 818, *pp.* 382–406.
doi:10.1017/jfm.2017.117

Unsteadily manipulating internal flow barriers

Sanjeeva Balasuriya†

School of Mathematical Sciences, University of Adelaide, Adelaide SA 5005, Australia

(Received 16 September 2016; revised 20 February 2017; accepted 20 February 2017; first published online 4 April 2017)

Typical flows contain internal flow barriers: specialised time-moving Lagrangian entities which demarcate distinct motions. Examples include the boundary between an oceanic eddy and a nearby jet, the edge of the Antarctic circumpolar vortex or the interface between two fluids which are to be mixed together in an microfluidic assay. The ability to control the locations of these barriers in a user-specified time-varying (unsteady) way can profoundly impact fluid transport between the coherent structures which are separated by the barriers. A condition on the unsteady Eulerian velocity required to achieve this objective is explicitly derived, thereby solving an 'inverse Lagrangian coherent structure' problem. This is an important first step in developing flow-barrier control in realistic flows, and in providing a postprocessing tool for observational/experimental velocity data. The excellent accuracy of the method is demonstrated using the Kelvin–Stuart cats-eyes flow and the unsteady double gyre, utilising finite-time Lyapunov exponents.

Key words: flow control, mixing, nonlinear dynamical systems

1. Introduction

Obtaining Lagrangian coherent structures (LCSs) from given Eulerian velocity data sets continues to be an important research area (Mezić *et al.* 2010; Allshouse & Thiffeault 2012; Froyland & Padberg-Gehle 2014; Ma & Bollt 2014; Allshouse & Peacock 2015*a*; Budišić & Thiffeault 2015; Haller 2015; Karrasch, Farazmand & Haller 2015; Onu, Huhn & Haller 2015; Balasuriya, Kalampattel & Ouellette 2016; Budišić *et al.* 2016; Hadjighasem *et al.* 2016; Haller *et al.* 2016; Schlueter-Kuck & Dabiri 2017). A primary reason for this is that LCSs have crucial importance in fluid transport (Shadden 2011; Peacock & Haller 2013; Samelson 2013; Haller 2015). In particular, the boundaries between LCSs at each instance in time separate the fluid into regions with different transport characteristics. The exact definition of such a boundary depends on the particular method being used; to remain general across all such methods, the terms 'transport barrier' or 'internal flow barrier' will be used here. (The commonly used term 'Lagrangian coherent structure' will be largely avoided from this point onwards to prevent confusion, since there is a specific definition of LCS introduced by Haller (2015) based on previous work (Haller & Yuan 2000; Haller 2011). Nowadays, the term LCS appears to be used for the entire range of techniques which seek structures (and their boundaries) from the Lagrangian

† Email address for correspondence: sanjeevabalasuriya@yahoo.com

advection of fluid parcels according to observed/specified Eulerian velocity fields.) The word 'internal' implies that these are barriers internal to the fluid, i.e. separating different regions of the fluid. For general unsteady Eulerian velocities, these flow barriers will generally themselves be moving in time.

This paper addresses the natural inverse question: given a specified time-varying flow barrier, is it possible to determine the Eulerian velocity field which would result in this Lagrangian entity? A condition on this Eulerian velocity will be derived under certain restrictions. This builds on preliminary work by Balasuriya & Padberg-Gehle (2014*b*), and is able to provide explicit velocity expressions in Eulerian coordinates. The efficacy of the method on synthetic data will be demonstrated.

Knowledge of the required Eulerian velocity offers a first step in a particular aspect of flow control: that of controlling Lagrangian flow barriers internal to the fluid. As such, it falls under the concept of Lagrangian flow control (Glass & Horsin 2010, 2012; Lei *et al.* 2015; Sinha, Vaidya & Rajaram 2016) in which the Lagrangian motion of fluid particles is to be controlled in a desired fashion. This may help address broader goals of flow control such as ensuring robust flow properties (Fish & Lauder 2006; Karnik *et al.* 2007; Kucala & Biringen 2014; Boujo, Fani & Gallaire 2015; Brunton & Noack 2015; Sattarzadeh & Fransson 2016; Tounsi *et al.* 2016) or enhancing or suppressing mixing (Ho & Tai 1998; Park *et al.* 2014; Cheikh & Lakkis 2016). The methods described in this paper are therefore from a different angle than more established flow control methods such as velocity modification based on flow sensing (Beebe *et al.* 2000; Jadhav *et al.* 2015; Frank *et al.* 2016; Tounsi *et al.* 2016), stabilising unstable or chaotic trajectories (Ott, Grebogi & Yorke 1990; Pyragas 1992; Boccaletti *et al.* 2000; Tamaseviciute *et al.* 2013), controlling autonomous vehicles by sampling fluid velocities (Senatore & Ross 2008; Mallory *et al.* 2013; Michini *et al.* 2014; Heckman, Schwartz & Hsieh 2015), designing optimal geometries for microfluidic devices (Ionov *et al.* 2006; Balasuriya 2015; Jeong *et al.* 2016), determining control velocities for energy/enstropy-constrained mixing (Mathew *et al.* 2007; Cortelezzi, Adrover & Giona 2008; Lin, Thiffeault & Doering 2011; Balasuriya & Finn 2012; Hassanzadeh, Chini & Doering 2014) and many others (Kim & Bewley 2007). Knowing the Eulerian velocities which engender a particular unsteady flow barrier can be used as a condition to build various control strategies: determining the optimal global Eulerian velocity to control flow barriers, finding a control forcing that must be applied, determining where to place flow actuators and when to invoke them, etc.

A second direction in which the methodology developed here offers an advance is in the postprocessing of observational or experimental Eulerian velocity data. In particular, if there is additional information on Lagrangian structures, this can be used to adjust the Eulerian velocities appropriately. An interesting example in this direction has been suggested for assimilating oceanographic sea-surface temperature front data into correcting Eulerian velocity fields obtained from sea-surface height measurements (Gaultier *et al.* 2013, 2014). The Eulerian velocities as obtained in the current paper offer quick expressions for making such an adjustment. More broadly, the methodology provides a new tool that can be used to postprocess Eulerian data to result in certain types of Lagrangian adjustments.

This article is organised as follows. Section 2 outlines and provides a solution to the problem of determining an Eulerian velocity field which results in prescribed Lagrangian flow barriers. Arbitrary time variation can be specified on these. Section 3 demonstrates excellent numerical validation using steady (Kelvin–Stuart cats-eyes in § 3.1) and unsteady (double gyre in § 3.2) models for the data. Section 4 discusses

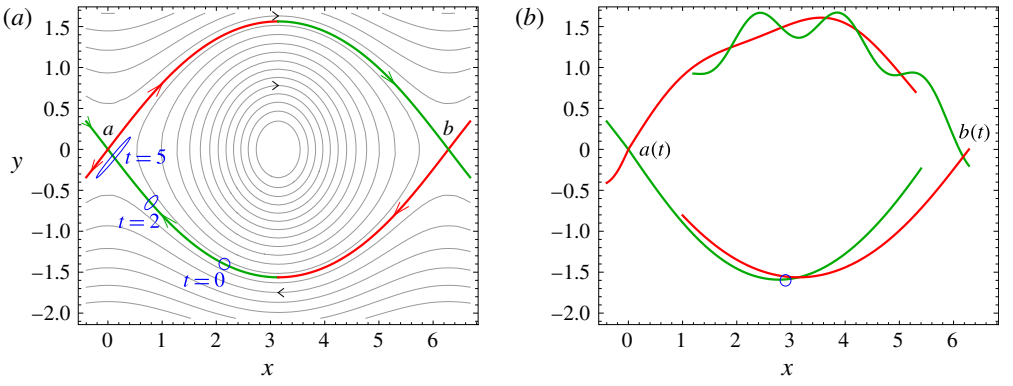

FIGURE 1. (Colour online) A well-defined internal flow barrier for an unsteady flow is shown in (*a*) and its counterpart (at a general time t) in an unsteady situation in (*b*).

the possibility of extending the information on the Eulerian velocity to determine a driving force which will lead to the required Lagrangian structures. Finally, § 5 outlines how the methods described here can be used as a first step for more refined flow control and data postprocessing applications.

2. Eulerian velocity for obtaining specified Lagrangian flow barriers

2.1. *Flow barriers: unsteadiness and finite-time issues*

This subsection establishes some insights into flow barriers, to help explain the development in the next subsection. A simple transport barrier for a steady flow is illustrated in figure 1(*a*), which shows the streamlines of the classical Kelvin–Stuart cats-eyes flow (Stuart 1967; Sharma & McKeon 2013). The distinguished red/green curves clearly represent the barriers between the vortex and the upper and lower jets, all three of which can be interpreted as coherent in the sense of Lagrangian particle trajectories of the flow $\dot{\boldsymbol{x}} = \boldsymbol{v}(\boldsymbol{x})$, where $\boldsymbol{v}$ is the steady Eulerian velocity field. Manipulating these flow barriers, which are internal to the fluid, in a specified time-varying way will therefore be a method for controlling transport between the coherent structures.

Unfortunately, the straightforward flow-barrier interpretation for the steady flow of figure 1(*a*) becomes less clear in an unsteady situation. However, barriers can be rationalised in terms of extremal stretching of fluid elements, as can be argued from the steady picture of figure 1(*a*). As the blue fluid element at time $t = 0$ evolves, it approaches the stagnation point $\boldsymbol{a}$ and gets pulled apart in the direction of the red arrows while compressing in to $\boldsymbol{a}$. The green curve it straddles is the stable manifold of $\boldsymbol{a}$, comprising fluid particles which approach $\boldsymbol{a}$ in the limit $t \to \infty$, while the red curve which influences its stretching is the unstable manifold of $\boldsymbol{a}$. Stable and unstable manifolds are now well established in the dual role of being associated with flow barriers and yet engendering transport between coherent structures through their potential tangling (Rom-Kedar, Leonard & Wiggins 1990; Wiggins 1992; Franco *et al.* 2007; Haller 2015; Balasuriya 2016*a*). Red and green will respectively be used for unstable and stable manifolds throughout this paper; the fact that the flow barriers are coloured with both red and green in figure 1(*a*) is a consequence of the fact that, for example, the unstable manifold of $\boldsymbol{a}$ coincides with the stable manifold of $\boldsymbol{b}$,

thereby forming an indubitable flow barrier. The stretching occurs at an exponential rate as a consequence of the fact that flow near the saddle stagnation point $\boldsymbol{a}$ is approximated by $\dot{\boldsymbol{x}} = \nabla \boldsymbol{v}(\boldsymbol{a})\boldsymbol{x}$, with the eigenvectors corresponding to the negative and positive eigenvalues of $\nabla \boldsymbol{v}(\boldsymbol{a})$ defining the local stable and unstable manifold emanation directions respectively. Thus, fluid elements straddling a stable manifold will stretch exponentially in forward time, and the two ends of the elongated fluid element will get pushed rapidly into the two different coherent structures. Similarly, fluid elements straddling an unstable manifold will stretch exponentially in backward time. Put another way, stable manifolds are flow barriers in forward time, while unstable manifolds are flow barriers in backward time.

The advantage of the above statement (in contrast with some other properties of stable/unstable manifolds) is that it remains legitimate for unsteady flows, as illustrated in figure 1(*b*), which shows stable (green) and unstable (red) manifolds emanating from two anchoring points $\boldsymbol{a}(t)$ and $\boldsymbol{b}(t)$, at an instance in time t. Once again, the fate of the blue fluid element straddling the stable manifold must be similar to before: it approaches $\boldsymbol{a}(t)$ as time increases and gets stretched out by the unstable manifold. This is irrespective of the nature of the intersection pattern; for example in figure 1(*b*) it is irrelevant that this element also intersects the unstable manifold of $\boldsymbol{b}(t)$. An important difference from the steady situation pictured in figure 1(*a*), however, is the fact that neither the manifolds nor the anchor points are stationary. (The time-varying anchor points are actually specialised trajectories – hyperbolic trajectories – of the flow, whose control has recently been pursued (Balasuriya & Padberg-Gehle 2013, 2014*a*).) In spite of this, the forward- and backward-time separating properties of the unsteady stable and unstable manifolds remain true. This is why forward-time finite-time Lyapunov exponent (FTLE) fields (Shadden, Lekien & Marsden 2005; Senatore & Ross 2008; Tallapragada & Ross 2013; Kucala & Biringen 2014; Raben, Ross & Vlachos 2014; Allshouse & Peacock 2015*b*; BozorgMagham, Ross & Schmale 2015; Haller 2015; Balasuriya *et al.* 2016), which measure exponential stretching, reveal strong ridges along stable manifolds and backward-time FTLE fields along unstable manifolds. In spite of the intersections possibilities between the manifolds, the following characteristic remains true for unsteady flows: stable manifolds are flow barriers in forward time, while unstable manifolds are flow barriers in backward time. Thus, having these move in ways which are prescribed is a first step in controlling fluid transport between coherent structures.

Defining stable and unstable manifolds, however, requires knowing the Eulerian velocity field over infinite times. This is clearly unfeasible in any realistic finite-time situation. Different diagnostic methods (of which FTLEs is one) seek entities which generalise stable/unstable manifolds in some way, or possess characteristics which are similar to those. While giving an extensive review on these is beyond the scope of this paper, since the idea here is to control such finite-time flow barriers, a discussion on some of these diagnostic methods is given in appendix A.

For this work, the following understanding suffices for stable/unstable manifold proxies (i.e. flow barriers) for general flows

$$\dot{\boldsymbol{x}} = \boldsymbol{v}(\boldsymbol{x}, t), \tag{2.1}$$

in two dimensions defined over a finite-time interval $[-T, T]$. Necessary (but not sufficient) conditions for a time-varying curve $\Lambda(t)$ to be a stable manifold proxy (SMP) for (2.1) for times $t \in (-T, T)$ are:

(i) the definition of $\Lambda(t^\star)$ will depend on behaviour of (2.3) for times $t \in [t^\star, T]$;

(ii) there is a neighbourhood around $\Lambda(t^\star)$ such that if a fluid element e were chosen in this neighbourhood, the following is true: the distance between the Lagrangian evolution of both e and $\Lambda(t^\star)$ from time $t^\star$ onwards, increases with time (i.e. $\Lambda(t^\star)$ is repelling);
(iii) the above property is true at all choices of times $t^\star$ in $(-T, T)$, implying that $\Lambda(t)$ is a genuinely unsteady entity in this interval (and not just defined at a fixed time $t^\star$);
(iv) moreover, $\Lambda(t)$ is Lagrangian; it is a material curve of (2.1).

Beyond these conditions, a specific proxy will not be chosen. However, it is noted that these conditions are shared by FTLEs and hyperbolic LCSs. Similarly, necessary (but not sufficient) conditions for a time-varying curve $\Lambda(t)$ to be a unstable manifold proxy (UMP) for (2.1) for times $t \in (-T, T)$ are:

(i) the definition of $\Lambda(t^\star)$ will depend on behaviour of (2.3) for times $t \in [-T, t^\star]$;
(ii) there is a neighbourhood around $\Lambda(t^\star)$ such that if a fluid element e were chosen in this neighbourhood, the following is true: the distance between the Lagrangian evolution of both e and $\Lambda(t^\star)$ from time $t^\star$ onwards, decreases in time (i.e. $\Lambda(t^\star)$ is attracting);
(iii) the above property is true at all choices of times $t^\star$ in $(-T, T)$, implying that $\Lambda(t)$ is a genuinely unsteady entity in this interval (and not just defined at a fixed time $t^\star$);
(iv) moreover, $\Lambda(t)$ is Lagrangian; it is a material curve of (2.1).

2.2. *Control velocity*

The control velocity problem and its solution can now be stated. Suppose two-dimensional Eulerian velocity data are available on a spatial grid, at discrete times, over a time interval $(-T, T)$. The data will typically be in the form $\boldsymbol{u}_{ij} = \boldsymbol{u}(\boldsymbol{x}_i, t_j)$, with the i representing the grid points and the j the temporal sampling. Lagrangian trajectories therefore obey

$$\dot{\boldsymbol{x}} = \boldsymbol{u}(\boldsymbol{x}, t), \tag{2.2}$$

whose implementation will require appropriate interpolation of the data. It will be assumed that the system (2.2) has a flow barrier – either a SMP or a UMP – $\tilde{\Gamma}(t)$ for each t in the time domain. If a SMP, it could for example be a strong ridge of the forward-time FTLE field generated by beginning at time t, or a curve from which there is locally maximal repulsion (if using the concept of hyperbolic LCSs of Haller (2015)). The question is the following: given a prescribed flow barrier $\Gamma(t)$ which is close to $\tilde{\Gamma}(t)$, what is the Eulerian velocity adjustment $\boldsymbol{c}(x, t)$ that needs to be added to (2.2) in order for the system to generate $\Gamma(t)$ as a Lagrangian flow barrier? Putting it another way: is it possible to determine the control velocity $\boldsymbol{c}$ in

$$\dot{\boldsymbol{x}} = \boldsymbol{u}(\boldsymbol{x}) + \boldsymbol{c}(\boldsymbol{x}, t), \tag{2.3}$$

such that (2.3) possesses the time varying $\Gamma(t)$ as a flow barrier?

This question can be answered under certain conditions. The first is that (2.2) is a flow in which the unsteadiness is not too dominant: $\boldsymbol{u}_{ij}$ changes little with j. Define the steady velocity

$$\bar{\boldsymbol{u}}_i = \bar{\boldsymbol{u}}(\boldsymbol{x}_i) = \langle \boldsymbol{u}(\boldsymbol{x}_i, t_j) \rangle, \tag{2.4}$$

by simply averaging over time, and the corresponding steady flow

$$\dot{\boldsymbol{x}} = \bar{\boldsymbol{u}}(\boldsymbol{x}). \tag{2.5}$$

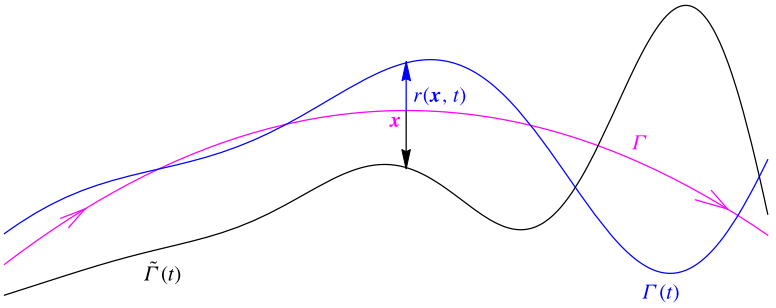

FIGURE 2. (Colour online) Original flow barrier $\tilde{\Gamma}(t)$ (black) of (2.2), steady manifold Γ (magenta) of (2.5) and required unsteady flow barrier $\Gamma(t)$ (blue) of (2.3) at a time instance t; $r(\boldsymbol{x}, t)$ is specified at each location $\boldsymbol{x} \in \Gamma$ as the displacement in the direction $\hat{\boldsymbol{n}}$.

Since (2.5) is steady, it can be considered a dynamical system for all (infinite) times. Suppose that (2.5) has a flow barrier (in this case precisely a stable or an unstable manifold) Γ. It will be necessary that the flow barriers Γ, $\tilde{\Gamma}(t)$ and $\Gamma(t)$ are all of the same type (i.e. either all SMPs or all UMPs). The specification of $\Gamma(t)$ shall be assumed to be given as in figure 2. At any point $\boldsymbol{x} \in \Gamma$, $\bar{\boldsymbol{u}}(\boldsymbol{x})$ is tangential to Γ. By defining the 90°-rotation operator $(x_1, x_2)^{\perp} := (-x_2, x_1)$ componentwise for vectors in $\mathbb{R}^2$, it is clear that a unit normal vector to Γ at $\boldsymbol{x}$ is given by $\hat{\boldsymbol{n}}(\boldsymbol{x}) := \bar{\boldsymbol{u}}(\boldsymbol{x})^{\perp}/|\bar{\boldsymbol{u}}(\boldsymbol{x})|$. The required time-varying manifold $\Gamma(t)$ is defined by specifying the displacement $r(\boldsymbol{x}, t)$ along the direction $\hat{\boldsymbol{n}}(\boldsymbol{x})$ at each location $\boldsymbol{x}$ on Γ, and at each time t, as shown in figure 2. The prescribed r shall be assumed to be small and suitably smooth adjacent to Γ. A specification of the required manifold is thus given by

$$\Gamma(t) := \{\boldsymbol{x} + r(\boldsymbol{x}, t)\hat{\boldsymbol{n}}(\boldsymbol{x}) : \boldsymbol{x} \in \Gamma\}, \tag{2.6}$$

valid in whatever part of Γ, and for whatever times t, required. This is a 'normal mappability' condition from $\Gamma(t)$ to Γ at all times, and a similar mappability is assumed between $\tilde{\Gamma}(t)$ and Γ.

It is shown in appendix B that the control velocity needs to satisfy the condition

$$\boldsymbol{c} = \bar{\boldsymbol{u}} - \boldsymbol{u} + \left\{ \frac{\partial r}{\partial t} + \bar{\boldsymbol{u}} \cdot \nabla r - \frac{\bar{\boldsymbol{u}} \cdot [(\nabla \bar{\boldsymbol{u}})\bar{\boldsymbol{u}}]}{|\bar{\boldsymbol{u}}|^2} r \right\} \frac{\bar{\boldsymbol{u}}^{\perp}}{|\bar{\boldsymbol{u}}|} + \{[(\nabla \bar{\boldsymbol{u}})\bar{\boldsymbol{u}}]^{\perp} - (\nabla \bar{\boldsymbol{u}})\bar{\boldsymbol{u}}^{\perp}\} \frac{r}{|\bar{\boldsymbol{u}}|}, \tag{2.7}$$

on Γ. To achieve $\Gamma(t^\star)$ at a time $t^\star$, it is necessary that (2.7) be satisfied for $t \geqslant t^\star$ if $\Gamma(t)$ is a SMP or for $t \leqslant t^\star$ if a UMP. The accumulated effect of the control velocity $\boldsymbol{c}$ over time results in the appropriate manifold proxy $\Gamma(t^\star)$ at time $t^\star$. To achieve $\Gamma(t)$ for $t \in [-T, T]$, then, (2.7) needs to be obeyed for all $t \in [-T, T]$. Therefore, flow barriers varying continuously according to a specification can be achieved.

With regards to the spatial variation, the derivation in appendix B indicates that (2.7) needs to be satisfied on Γ, and be extended continuously in space. An easily stated approach would be define $\boldsymbol{c}(\boldsymbol{x}, t)$ specifically by the formula (2.7) in a strip around Γ (this might be the easiest approach if using for data postprocessing). Another would be to have (2.7) define $\boldsymbol{c}(\Gamma, t)$, but to extend this into a strip in a continuous way while ensuring that any other required conditions are satisfied. For example, incompressibility can be satisfied since the condition is on $\boldsymbol{c}(\Gamma, t)$ at any time t, and thus this imposes conditions on the tangential (to Γ) and normal components of $\boldsymbol{c}$, and

also the tangential derivative of the tangential component. An extension can then be performed in the normal direction by insisting that the normal derivative of the normal component is negative the tangential derivative of the tangential component, thereby ensuring that incompressibility is satisfied. Any alternative extension – subject to a required physical constraint or based on realisability, say – is also possible. Having extended $\boldsymbol{c}$ to a strip in whatever way, it can be clipped to zero outside the strip; smoothness is only required near Γ. Also note that several manifold segments in a flow can be simultaneously manipulated by applying the velocity (2.7) in local strips around each such manifold.

Some intuition on the terms appearing in (2.7) may be welcome. The first two terms in the second row of (2.7) give the material derivative of $\boldsymbol{r}$ with respect to (2.2); this captures the fact that as time progresses, particles on Γ will travel along it according to (2.2), and thus r will be different at such locations. The term associated with the first bracket in (2.7) is guaranteed to be a velocity in the direction normal to Γ. Thus, in achieving this normal displacement, the second bracket term reveals that a tangential component of velocity might be needed. (Intuitively, the terms in these second brackets capture the curvature of Γ.) The presence of such a tangential term is not surprising, since purely normal Eulerian velocities give tangential displacements of Lagrangian manifolds (Balasuriya 2011). The present context is the inverse of this: a purely normal Lagrangian manifold displacement requiring a tangential Eulerian velocity component.

While the development in appendix B is formal in nature, it relies on properties of SMPs/UMPs, the displacement $|r|$ and the unsteadiness $|\boldsymbol{u} - \bar{\boldsymbol{u}}|$ being small, and is valid in regions and times where both $\tilde{\Gamma}(t)$ and $\Gamma(t)$ are normally mappable to Γ. Based on rigorous results (Balasuriya & Padberg-Gehle 2014*b*) from a different (and not easily implementable) perspective, the error in using (2.7) to obtain $\Gamma(t)$ is expected to be of second order in these quantities. Note moreover that the details of the flow barrier $\tilde{\Gamma}(t)$ of the original flow are not required in defining (2.7); its existence is all that is needed.

The intersection pattern between stable and unstable manifolds at a given instance in time is well known to strongly influence fluid mixing (Rom-Kedar *et al.* 1990; Franco *et al.* 2007; Balasuriya 2016*a*). A classical method of imparting mixing is to apply an unsteady velocity perturbation to a steady situation such as figure 1(*a*), which results in the coincident stable and unstable manifolds splitting apart (for example like figure 1*b*). An interesting question in attempting to control the transport across such a broken connection would therefore be whether it was possible to separately manipulate the stable and unstable manifolds. So, for example, transport between the inside of the vortex and the upper region in figure 1(*a*) might be controlled by manipulating the locations of the upper red (unstable) and green (stable) curves in figure 1(*b*), at some time $t^\star$. Since (2.7) would need to apply for $t > t^\star$ for the stable manifold and $t < t^\star$ for the unstable manifold, the relevant velocities can be separately specified to achieve this.

3. Numerical validation

3.1. *Kelvin–Stuart cats-eyes flow*

The accuracy of the method is first illustrated for the Kelvin–Stuart cats-eyes flow pictured in figure 1(*a*). The steady Kelvin–Stuart flow – an exact solution to the Euler equations – is given by the velocity field (Stuart 1967; Sharma & McKeon 2013;

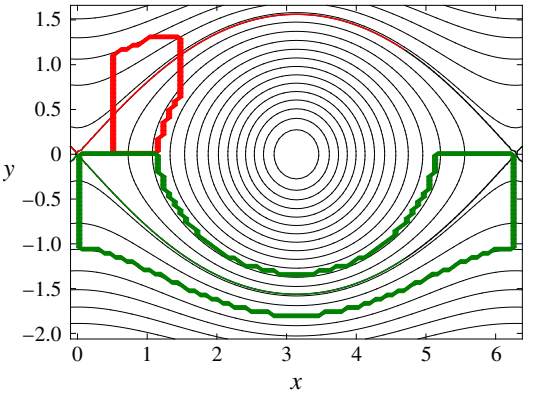

FIGURE 3. (Colour online) The regions (heavy curve boundaries) in which the control velocity (2.7) is to be applied with respect to moving the unstable (red) and stable (green) manifolds.

Balasuriya 2016*a*)

$$\boldsymbol{u}(x, y) = \left(\frac{b \sinh y}{b \cosh y + \sqrt{b^2 - 1} \cos x}, \frac{\sqrt{b^2 - 1} \sin x}{b \cosh y + \sqrt{b^2 - 1} \cos x} \right), \tag{3.1}$$

where $b > 1$ is a parameter and $\boldsymbol{x} = (x, y)$. The initial focus will be on the unstable and stable manifolds emanating from (0, 0) into the first and fourth quadrants in figure 1(*a*), which are given by $y = \pm \cosh^{-1}[1 + \sqrt{b^2 - 1}(1 - \cos x)/b]$, and are shown by thin red and green curves respectively in figure 3. Suppose a time-varying bulge is to applied in the normal direction to the unstable manifold, given by the expression

$$r_u(x, y, t) = \varepsilon \left[20 \cos t \left(x - \tfrac{1}{2} \right)^2 \left(x - \tfrac{3}{2} \right)^2 \right] \mathbb{1}_{(1/2, 3/2)}(x), \tag{3.2}$$

where ε is a small parameter and $\mathbb{1}$ is the indicator function (taking the value one when the argument is in the indicated domain, zero otherwise). Simultaneously, suppose that the stable manifold is desired to be moved according to the time-aperiodic specification

$$r_s(x, y, t) = \varepsilon \left[(1 + \tanh t) \tanh \frac{x}{5} \right]. \tag{3.3}$$

It is now straightforward to compute the values of the control velocity $\boldsymbol{c}$ associated with each of these manifold deviations using (2.7). In particular, since the original flow is steady, $\boldsymbol{u}(\boldsymbol{x}, t) = \bar{\boldsymbol{u}}(\boldsymbol{x})$ and the terms in the first line disappear. In this example, suppose the expression given specifically by (2.7) is used to define $\boldsymbol{c}(\boldsymbol{x}, t)$ in regions around the relevant manifold as demarcated by the thick curves in figure 3. Care should be taken to ensure that the required manifold deviations remain within these regions; thus the width of the regions should be large enough depending on the value of ε. This enables the control velocity to be defined for all times, and numerical experimentation is possible.

The process of comparing the results to the desired manifold variation at any time t is as follows. The full velocity (Kelvin–Stuart plus the control velocity as computed

above) is used for numerical particle advection beginning at time t. Backward FTLE fields are computed within the domain shown in figure 3; the strong ridges of these, adjacent to the thin red curve in figure 3, will numerically determine the UMP at that instance in time. The time of advection used in this process is an important parameter. Longer segments of the unstable manifold emanating from $(0, 0)$ can be captured by increasing this time of advection, but this means that other unstable manifolds will also emerge as ridges of the backward FTLE field. For example, the green curve in figure 3 is a SMP of $(0, 0)$, but since it is also a UMP of the hyperbolic trajectory near $(2\pi, 0)$ this will also emerge as a ridge of the backward FTLE field, but will be connected to the right hyperbolic trajectory. On the other hand, computing forward FTLE fields (by advecting particles forward in time from t) will reveal SMPs.

Figure 4 shows the results of this comparison where the manifold deviation parameter has been chosen to be $\varepsilon = 0.2$ and a time of advection of 12 is used throughout. Forward and backward FTLE fields are shown at several different times, and the desired flow barrier locations at those times, as given by (3.2) and (3.3), are indicated by the thin red (UMP) and green (SMP) curves superimposed on the same figures. The results are excellent. Tests at other t values also indicated very good agreement. Even better agreement results if using smaller ε (not shown). Several time-varying flow-barrier deviations which are different to (3.2) and (3.3) were analysed; usage of the relevant control velocity using (2.7) once again gave excellent results (not shown).

Next, consider forcing transport into the cats-eyes eddy from the lower jet, by splitting the lower coincident stable/unstable manifold in figure 1. Thus, the same SMP as considered in the previous numerical experiments shall be used, with deviation given by $\tilde{r}_s = r_s$ as given by (3.3). The unperturbed unstable manifold is the same entity, but now suppose that it is required to deviate this by $\tilde{r}_u(x, y, t) = -r_s(2\pi - x, y, t)$. This sign ensures that the SMP and UMP at a given time t split in opposite directions, thereby creating a channel along which fluid will transport from the lower jet to the eddy. Once again, the relevant control velocity can be computed using (2.7), and now it is sufficient to use the green region from figure 3 since the action is only in this region. The resulting FTLE fields at time 0 with $\varepsilon = 0.5$ is shown in figure 5. The agreement between the UMPs (red) and SMPs (green) with the relevant ridge of the backward (a) and forward (b) FTLE fields is excellent, even at this significant value of ε. The 'other' manifold proxy is also shown in each figure to show that the required splitting has been achieved, and since the flow in the region in between is from right to left, fluid will become entrained into the eddy from the lower jet. This is a uni-directional transport caused by the SMP and UMP not intersecting at time zero. (A time-dependent transport quantification of this form is possible for any intersecting/non-intersecting pattern between such manifolds (Balasuriya 2016*a*,*c*), which generalises the classical lobe dynamics approach (Rom-Kedar *et al.* 1990; Franco *et al.* 2007) to arbitrary time variation with or without lobes.) This behaviour has been created by design, showing the potential of the control methodology to control transport between coherent structures. Note that this required separate specifications of the control velocity in the times $t < 0$ and $t > 0$, to respectively control the unstable and the stable manifolds. Controlling both the stable and unstable manifolds over a range of time does not seem possible, since if controlling at a time $t^\star$, separate specifications for $t < t^\star$ and $t > t^\star$ would be necessary. If control is to be also achieved at a different $t^\star$ (call it $\tilde{t} < t^\star$), this will result in ambiguity of the control velocity definitions in the range $[\tilde{t}, t^\star]$. It may, however, be possible to control the transport as a function of time, even if the individual manifolds cannot.

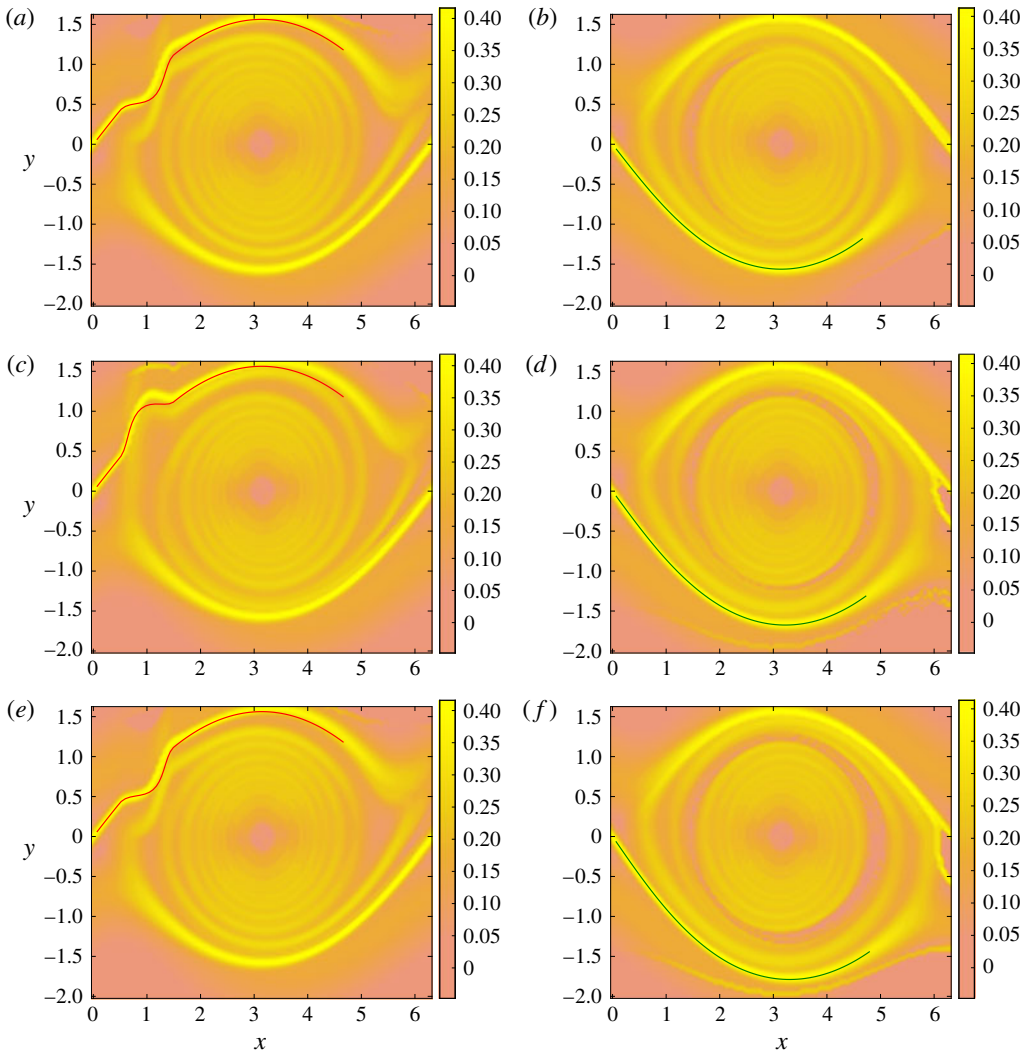

FIGURE 4. (Colour online) Backward (*a*,*c*,*e*) and forward (*b*,*d*,*f*) FTLE fields associated with the controlled Kelvin–Stuart flow with $b = 1.5$ and $\varepsilon = 0.2$, at $t = -3$ (*a*,*b*), 0 (*c*,*d*), and 3 (*e*,*f*). The required flow barriers are superimposed as thin red (unstable) and green (stable) curves.

3.2. *Controlling the unsteady double gyre*

Next, an example with unsteady data is considered. In keeping with a system whose behaviour is well understood, the unsteady double gyre introduced by Shadden *et al.* (2005) will be used to produce the data for the uncontrolled system. This obeys

$$\left.\begin{aligned} \dot{x} &= -\pi A \sin[\pi\phi(x,t)]\cos[\pi y], \\ \dot{y} &= \pi A \cos[\pi\phi(x,t)]\sin[\pi y]\frac{\partial\phi}{\partial x}, \end{aligned}\right\} \tag{3.4}$$

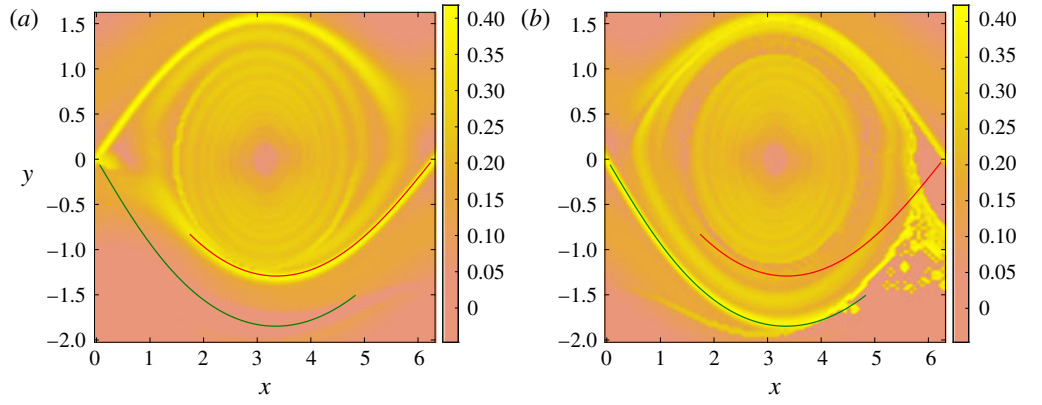

FIGURE 5. (Colour online) Backward (a) and forward (b) FTLE fields at $t = 0$ associated with splitting the lower coincident stable/unstable manifold into non-intersecting curves to enable transport from the lower jet to the eddy, with parameters $b = 1.5$ and $\varepsilon = 0.5$.

where the function ϕ is defined by

$$\phi(x, t) = \delta \sin(\omega t)x^2 + [1 - 2\delta \sin(\omega t)]x. \tag{3.5}$$

The parameter δ is usually considered small, since if $\delta = 0$, the system (3.4) consists of two counter-rotating gyres in the cells $[0, 1] \times [0, 1]$ and $[1, 2] \times [0, 1]$. The flow barrier is then along $x = 1$, being simultaneously the stable manifold of the point $(1, 0)$ and the unstable manifold of $(1, 1)$. When $\delta \neq 0$, this barrier breaks apart into separate stable and unstable manifolds, which intersect infinitely often leading to chaotic transport between the left and the right gyre. Finite-time simulations of (3.4) are common using most of the proxies discussed in this paper for stable/unstable manifolds, and they all succeed in revealing the expected structure of the flow barriers (Shadden *et al.* 2005; Froyland & Padberg 2009; Allshouse & Peacock 2015*b*; Balasuriya 2016*a*).

Since the manifolds of (3.4) when $\delta \neq 0$ have infinitely many folds, and re-enter the boundary of the usual domain of definition $[0, 2] \times [1, 0]$ infinitely closely, controlling the global extent of these manifolds is a daunting task. This section will focus on controlling the part of the stable manifold emanating from near $(1, 0)$. In the absence of explicit expressions for the flow barriers, (analytical approximations for small δ in the vicinity of $x = 1$ are available even when $\sin(\omega t)$ in (3.5) is replaced by an arbitrary bounded time-varying function (Balasuriya 2016*a*)) a SMP will serve to help identify this manifold. The strongest yellow ridge of the forward-time FTLE fields shown in figure 6(*a*,*c*,*e*) indicate the beginnings of this SMP. The ridge has many subsequent folds which the FTLE struggles to capture at this particular choice of system and plotting parameters ($A = 1$ and $\omega = 15$ are chosen throughout). The foot of the SMP is moving around near $(1, 0)$; this represents the hyperbolic trajectory to which the SMP is attached. In all the FTLE calculations to be described in this section, a spatial grid of 200×100 points is used, with time steps of size 0.01 used for a time duration of $3(2\pi/\omega)$ units. Forward advection is performed using a third-order Runge–Kutta scheme.

The intention is to force the beginning part of the flow barrier to follow a prescribed time-varying behaviour, which will be specified by writing it in the form

$$x_s(y, t) = 1 + \varepsilon y \tanh(t) \quad \text{for } 0 < y < 0.9 \tag{3.6}$$

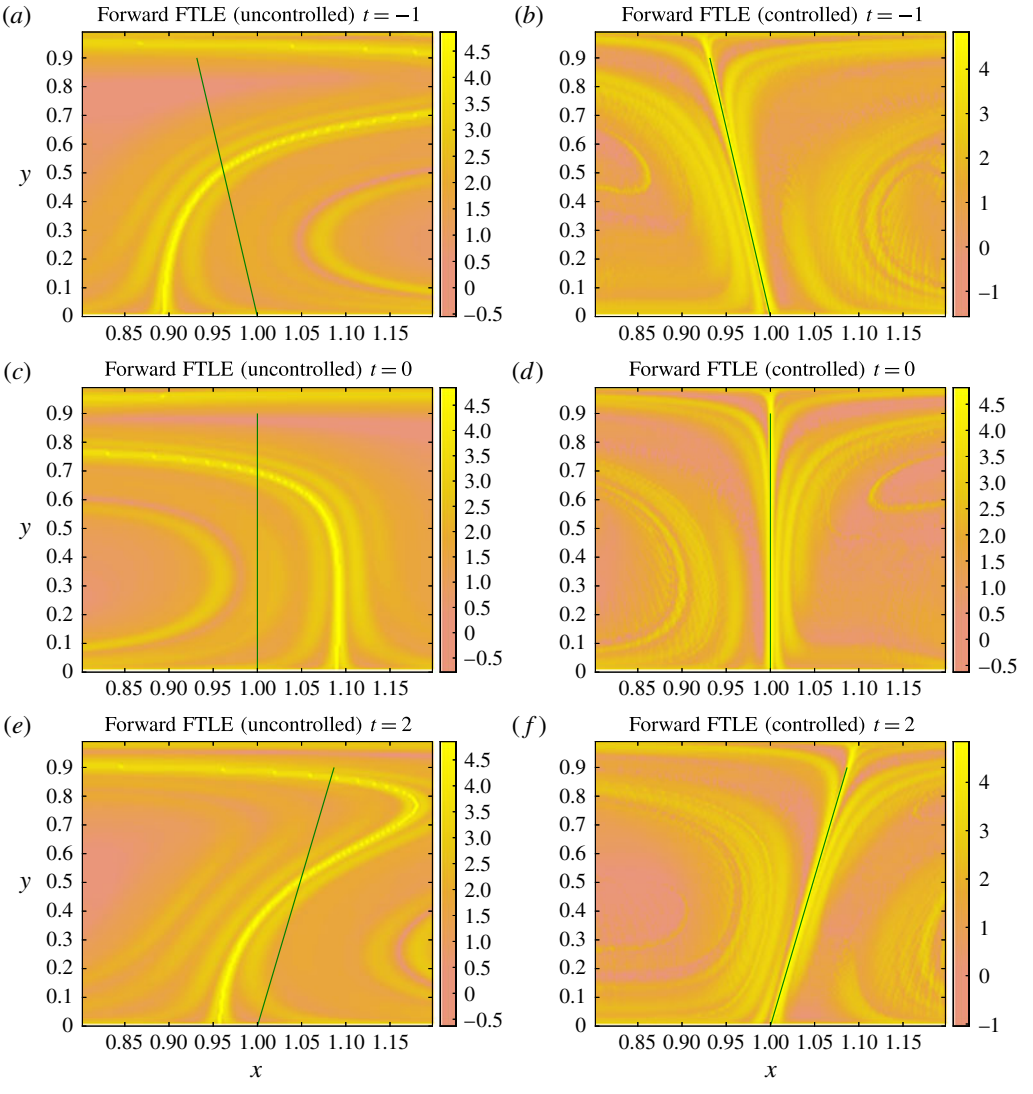

FIGURE 6. (Colour online) Forward-time FTLE fields for the uncontrolled (*a*,*c*,*e*) and controlled (*b*,*d*,*f*) double gyre subject to the prescription (3.6) at different times, with the desired SMP shown by the green curve. Here, $\delta = 0.2$, $\varepsilon = 0.1$ and $\eta = 0.2$.

for small $|\varepsilon|$. Going towards values close to $y = 1$ is clearly impossible since the flow barrier stretches and folds globally. Thus (3.6) is the prescribed SMP $\Gamma(t)$, which in this case is pinned at $(1, 0)$ and swivels from pointing into the left gyre to the right gyre as time progresses. Figure 6(*a*,*c*,*e*) indicates that the unsteady double-gyre flow of (3.4) clearly does not conform to this behaviour, and therefore a control mechanism must be applied.

To apply (2.7), the nearby steady velocity $\bar{\boldsymbol{u}}$ must be determined in the vicinity of $x = 1$. Now, the $\delta = 0$ steady flow seems like the obvious candidate, but this turns out to not be the flow arising from taking the time average (except when $\delta = 0$). While the time average of the data at each point (x, y) of (3.4) can be computed, in this

case an exact expression for the time average of (3.4) near $x=1$ over a time period $2\pi/\omega$ (the period of the flow) is given by

$$\left.\begin{aligned}\dot{x} &= \pi^2 A J_0(\pi\delta)\cos[\pi y](x-1),\\ \dot{y} &= -\pi A J_0(\pi\delta)\sin[\pi y],\end{aligned}\right\} \tag{3.7}$$

where J_0 is the Bessel function of the first kind (see appendix C). It was checked that the numerically averaging the data in a strip near $x=1$ did indeed converge to (3.7) for a suitably small strip and in the limit as the time step went to zero. A specific observation – either from the data or from (3.7) – is that $\dot{x}=0$ on $x=1$, which then is Γ, the stable manifold for the averaged steady system. For any given $r(y,t)$, it is shown in appendix C that the quantity $\boldsymbol{c}$ in (2.7) should be chosen to be

$$\boldsymbol{c}(y,t) = \bar{\boldsymbol{u}}(1,y) - \boldsymbol{u}(1,y,t) + \left[\frac{\partial r}{\partial t} - \pi A J_0(\pi\delta)\sin(\pi y)\frac{\partial r}{\partial y} - \pi^2 A J_0(\pi\delta)\cos(\pi y)s\right]\begin{pmatrix}1\\0\end{pmatrix}, \tag{3.8}$$

on $x=1$. In the specific case (3.6), r is given by

$$r(y,t) = \varepsilon y\tanh(t), \quad \frac{\partial s}{\partial t} = \varepsilon y\,\mathrm{sech}^2(t) \quad \text{and} \quad \frac{\partial r}{\partial y} = \varepsilon\tanh(t) \quad \text{for } 0<y<0.9, \tag{3.9a–c}$$

which can be inserted into (3.8). This velocity (3.8) will be applied uniformly in x, within the strip $x\in[1-\eta,1+\eta]$. To obtain a SMP at each given time $t^\star$, (3.8) needs to apply for all times $t\geqslant t^\star$. Only a finite time is being considered here, and thus the requirement needs to be met for times $t\in[t^\star, t^\star+3(2\pi/\omega)]$.

The controlled system is therefore (2.3) subject to the above identification of functions. Figure 6(*b*,*d*,*f*) indicates the forward-time FTLE fields obtained from the data associated with (3.9), with the choice $\varepsilon=0.1$ and $\eta=0.2$ (i.e. the control operates in the full strip shown in figure 6). There is a strong FTLE ridge lining up along the desired SMP (green curve). Comparing with (*a*,*c*,*e*), it is clear that the method has been outstandingly successful in moving the SMP in the desired time-varying fashion.

The parameter δ measures the level of unsteadiness present in the uncontrolled flow, and the method as developed assumed small δ and small deviation ε. To push the method beyond its originally designed framework, suppose $\delta=0.4$ and $\varepsilon=0.3$. Think of the unstable manifold emanating from near (1, 1) this time, and suppose it were required to pin it as

$$x_u(y,t) = 1+\varepsilon\sin(2\pi y) \quad \text{for } 0.1<y<1. \tag{3.10}$$

For this instance, the relevant r obeys

$$r(y,t) = \varepsilon y\sin(2\pi y), \quad \frac{\partial r}{\partial t}=0 \quad \text{and} \quad \frac{\partial s}{\partial y} = 2\pi\varepsilon\cos(2\pi y) \quad \text{for } 0.1<y<1. \tag{3.11a–c}$$

This value can be substituted into (3.8) to determine $\boldsymbol{c}$. While the bracketed term in (3.8) has no time dependence in this case, the presence of the $\bar{\boldsymbol{u}}-\boldsymbol{u}$ indicates that an unsteady control velocity applies in this instance in which a steady flow barrier is to be achieved. Moreover, in this instance if the required UMP is to be obtained at time $t^\star$, (3.8) must be obeyed at times $t\in[t^\star-3(2\pi/\omega), t^\star]$.

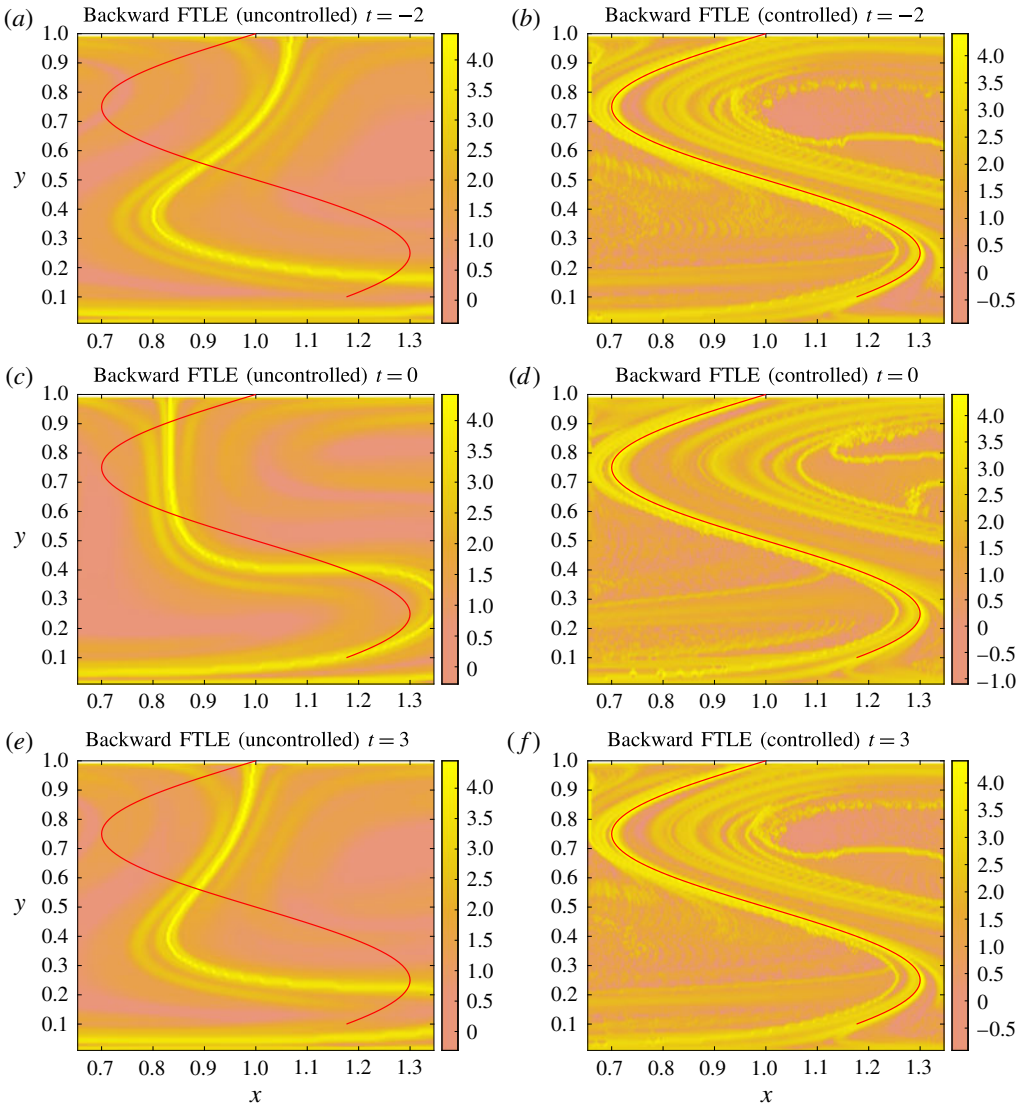

FIGURE 7. (Colour online) Backward-time FTLE fields for the uncontrolled (*a*,*c*,*e*) and controlled (*b*,*d*,*f*) double gyre subject to the prescription (3.10) at different times, with the desired UMP shown by the red curve. Here, $\delta = 0.4$, $\varepsilon = 0.3$ and $\eta = 0.35$.

With these new parameter choices in mind, figure 7 displays the comparison between the uncontrolled flow and the controlled one, in terms of backward-time FTLE fields, at several different choices of time. The required curve (red) in the left panels is seen to be very different from the uncontrolled unsteady double gyre. The controlled flow on the right indicates that there is a dominant FTLE ridge lying along the required red curve. In this controlled situation, (3.8) has resulted in many more (smaller) FTLE ridges than in the uncontrolled system, yet the dominant one clearly follows the required behaviour. Even with relatively large unsteadiness in the data, and required deviation, very good results are obtained.

4. Driving through Navier–Stokes

The examples above indicate that if the required Eulerian velocity as indicated by (2.7) were applied to a system, then excellent matching with prescribed Lagrangian flow barriers can be obtained. In this section, a brief commentary on the possibilities of achieving this Eulerian velocity via applying a driving force on the flow is presented. This shows one possible direction of utilising the methodology of this article in realistic flows. Is it possible to attain the requirement (2.7) by driving the Navier–Stokes equation by a force, which is more likely to be practically controllable? This is the question which led to the experimental investigations of Ouellette, Hogg & Liao (2016), who discovered a correlation between the probability of finding a SMP and the injected mean strain rate. Moreover, this concept is similar in spirit to the idea of driving the advection–diffusion equation to achieve a desired concentration developed by Sinha *et al.* (2016), though here the focus is on controlling the Lagrangian flow barriers by the forcing.

Section 2.2 developed a condition on the Eulerian velocity (2.7) required to generate a prescribed Lagrangian flow-barrier variation. Consider now the dynamics as being generated from the Navier–Stokes equations, and suppose that these internal flow barriers are well removed from boundaries. In stating this condition mathematically, it proves advantageous to define the two-dimensional scalar curl operator on functions $\boldsymbol{g}:\mathbb{R}^2\to\mathbb{R}^2$ by

$$\mathrm{rot}(\boldsymbol{g}) := \hat{\boldsymbol{k}}\cdot(\boldsymbol{\nabla}\times\boldsymbol{g}). \tag{4.1}$$

Then, the original vorticity $\mathrm{rot}(\boldsymbol{u})$ associated with the uncontrolled velocity in (2.2) will satisfy the non-dimensional vorticity equation

$$\frac{\partial \mathrm{rot}(\boldsymbol{u})}{\partial t} + \boldsymbol{u}\cdot\boldsymbol{\nabla}[\mathrm{rot}(\boldsymbol{u})] = \nu\nabla^2\mathrm{rot}(\boldsymbol{u}) + \mathrm{rot}(\boldsymbol{f}_u), \tag{4.2}$$

in which $\boldsymbol{f}_u$ is the body force associated with the equation and ν quantifies the viscosity. Moreover, $\boldsymbol{\nabla}\cdot\boldsymbol{u}=0$. Having $\boldsymbol{u}$ satisfy the Euler equations is also permitted by letting $\nu=0$. Thus, $\boldsymbol{u}$ will not merely be a kinematically defined velocity, but rather a solution of the Navier–Stokes (or Euler) equations.

The driven system will need to have the velocity field $\boldsymbol{u}+\boldsymbol{c}$, with $\boldsymbol{c}$ satisfying the condition (2.7). Is it possible to determine the driving in the Navier–Stokes equations that is required in order to generate precisely this velocity? The full vorticity equation will satisfy

$$\frac{\partial \mathrm{rot}(\boldsymbol{u}+\boldsymbol{c})}{\partial t} + (\boldsymbol{u}+\boldsymbol{c})\cdot\boldsymbol{\nabla}[\mathrm{rot}(\boldsymbol{u}+\boldsymbol{c})] = \nu\nabla^2\mathrm{rot}(\boldsymbol{u}+\boldsymbol{c}) + \mathrm{rot}(\boldsymbol{f}_u) + \mathrm{rot}(\boldsymbol{f}_c). \tag{4.3}$$

The additional body force $\boldsymbol{f}_c$ which needs to be supplied is therefore defined in terms of $\boldsymbol{c}$ by

$$\begin{aligned}\mathrm{rot}(\boldsymbol{f}_c) &= \frac{\partial \mathrm{rot}(\boldsymbol{u}+\boldsymbol{c})}{\partial t} + (\boldsymbol{u}+\boldsymbol{c})\cdot\boldsymbol{\nabla}[\mathrm{rot}(\boldsymbol{u}+\boldsymbol{c})] - \nu\nabla^2\mathrm{rot}(\boldsymbol{u}+\boldsymbol{c}) - \mathrm{rot}(\boldsymbol{f}_u)\\ &= \frac{\partial \mathrm{rot}(\boldsymbol{c})}{\partial t} + (\boldsymbol{u}+\boldsymbol{c})\cdot\boldsymbol{\nabla}[\mathrm{rot}(\boldsymbol{c})] + \boldsymbol{c}\cdot\boldsymbol{\nabla}[\mathrm{rot}(\boldsymbol{u})] - \nu\nabla^2\mathrm{rot}(\boldsymbol{c}).\end{aligned} \tag{4.4}$$

The above requirement needs to be satisfied on Γ. Moreover, the Navier–Stokes equations require the fluid to be incompressible, and thus an additional requirement on $\boldsymbol{c}$ is that $\boldsymbol{\nabla}\cdot\boldsymbol{c}=0$. Actual implementation of these conditions will depend on

the situation at hand. Since (4.4) is a condition on Γ, one issue would be how to continuously extend the force. A possible solution would be to extend the definition of $\boldsymbol{c}$ on Γ (a one-dimensional curve) in an incompressible way to a strip around Γ. This is possible because the condition (2.7) specifies the control velocity along a one-dimensional curve, allowing for the freedom to decide how to extend $\boldsymbol{c}$ in the direction normal to Γ. Then, (4.4) can be used to determine a condition on the forcing in this strip. Another interesting aspect is that (4.4) tells us information about the curl of the required force, but not the force itself. Many different forms of $\boldsymbol{f}_c$ can be chosen to satisfy this condition, and each of these is moreover only defined modulo an additive conservative force. Thus, it seems that there are several freedoms in determining the forms of body force on Γ, and its spatial extensions, which will eventually lead to the prescribed Lagrangian flow barriers.

5. Concluding remarks

A promising new approach which elucidates the control velocity (in Eulerian coordinates) required to have internal flow barriers move in a prescribed time-varying way has been developed in this article. This provides a methodology for controlling transport across such a barrier, that is, between coherent structures. The derivation (in appendix B) relies on previous rigorous results (Balasuriya & Padberg-Gehle 2014*b*) and the attracting property of flow barriers in the appropriate direction of time (Haller 2015). Since such attraction/repulsion is also the basis for a leading approach (hyperbolic Lagrangian coherent structures (Haller 2015)) in identifying transport barriers in flows whose velocities are only known for finite times, the method can also be adapted to such flows. It was shown via example that the method has excellent performance.

The main result is the determination of the control velocity needed to move an unsteady transport barrier to a (nearby) prescribed unsteady one. This is an essential first step in the broader topic of being able to control transport barriers. It can, for example, be used as a constraint in developing optimal control methodologies which minimise energy; having this information on the required velocity in Eulerian conditions is highly useful in such additional steps.

A novel application of this method could also be the issue of correcting for oceanographic velocity data, which are usually obtained from satellite measurements of sea-surface height (SSH). There are many issues in obtaining accurate values of oceanic velocities: the poor resolution ($\sim$100 km), measurement inaccuracies, errors resulting from using the geostrophic approximation to convert sea-surface heights to velocities, etc. Gaultier *et al.* (2013, 2014) propose using additional data such as sea-surface temperature (SST), whose evolution is governed by fluid parcels travelling in a Lagrangian way according to oceanic velocities, to correct these velocities. Fronts of the SST field would presumably be aligned with transport barriers imputed from the SSH-generated oceanic velocities, and this is indeed approximately observed (Gaultier *et al.* 2013, 2014). Now, if treating the SST fronts as the truth (i.e. actual transport barriers), the relevant normal displacement of the SSH-generated transport barriers (using one's favourite LCS approach) can be determined using the data. This, then, can be used as the r in (2.7), and the $\boldsymbol{c}$ would correspond to the velocity correction that needs to be applied in order to get the correct transport barriers. Initial work on this approach has begun. Data assimilation approaches, say by introducing the condition (2.7) into a cost function, can then be developed.

It must be emphasised that what has been presented is the first step – determining an Eulerian velocity which generates required/observed Lagrangian flow barriers

– in the longer-term development of a robust control strategy for unsteady flow barriers. The condition (2.7) has not been known until now. The extension to determining the requirement (4.4) on a driven Navier–Stokes equation also offers a new tool for designing realistic flow barriers. It is anticipated that this basic and essential information will be incorporated into future developments of optimal methods of controlling flow barriers, or otherwise optimally utilising information for postprocessing data.

Acknowledgement

Support from the Australian Research Council through Future Fellowship grant FT130100484 is gratefully acknowledged.

Appendix A. Diagnostic methods for flow barriers

For convenience, the understanding of $\Lambda(t)$ as a proxy for a stable manifold of a general system (2.1) will be first discussed.

(i) *Infinite-times:* if the velocity field is defined for infinite times (as is technically necessary to specifically define stable/unstable manifolds), then fluid particles on $\Lambda(t^\star)$ will approach a hyperbolic trajectory of (2.3) as $t \to \infty$. A hyperbolic trajectory is the unsteady analogue of a hyperbolic stagnation point, and whose technical definition involves the concept of exponential dichotomies (Coppel 1978; Balasuriya 2012; Balasuriya & Padberg-Gehle 2014*a*) which is beyond the scope of the present article. Intuitively, it is a time-varying trajectory of (2.3) to which is attached time-varying one-dimensional stable and unstable manifold curves, representing particles which approach it exponentially in forward/backward time respectively. In this case, $\Lambda(t^\star)$ would be the stable manifold curve attached to the hyperbolic trajectory at the time instance $t^\star$. As time evolves, the hyperbolic trajectory will move, as will this curve; this generates the time variation $\Lambda(t)$.

(ii) *FTLEs:* a frequently used proxy for finite times is that of a finite-time Lyapunov exponent ridge (Shadden *et al.* 2005; Senatore & Ross 2008; Tallapragada & Ross 2013; Kucala & Biringen 2014; Raben *et al.* 2014; Allshouse & Peacock 2015*b*; BozorgMagham *et al.* 2015; Haller 2015; Balasuriya *et al.* 2016). The analogue of a stable manifold is a forward-time FTLE ridge, representing curves such that if fluid elements were placed on them at time $t^\star$, they would experience anomalously large exponential stretching for times $t \in [t^\star, T]$ in comparison to nearby elements.

(iii) *Hyperbolic LCSs:* a rigorous theory (Haller & Yuan 2000; Haller 2011, 2015; Haller & Beron-Vera 2012; Blazevski & Haller 2014) exists for the concept of a repelling hyperbolic Lagrangian coherent structure, a finite-time analogue of a stable manifold. These are obtained from (2.3) by seeking curves at time $t^\star$ from which there is maximal repulsion by the flow when applied in the time $[t^\star, T]$ (Karrasch *et al.* 2015; Onu *et al.* 2015). An important ingredient in the theory is the insistence that these curves are Lagrangian entities; that is, if the solutions to this maximal repulsion problem are considered at different times $t^\star$, then the relevant entities obtained are material curves of (2.3).

(iv) *Lagrangian averages:* scalar fields can be defined by taking Lagrangian averages of the flow of (2.3) over the finite time domain $[t^\star, T]$ (Mezić *et al.* 2010; Mancho *et al.* 2013; Budišić *et al.* 2016; Haller *et al.* 2016). Sharp transitions in these fields are often linked to stable manifold proxies.

(v) *Transport-based proxies:* another class of methods examines transport occurring from time $t^\star$ to T using transition matrices (Perron–Frobenius operators), with

diffusion implicitly or explicitly incorporated in the numerical method (Froyland & Padberg 2009; Froyland, Santitissadeekorn & Monahan 2010; Froyland 2013; Froyland & Padberg-Gehle 2014). Sharp transitions in eigenfunctions associated with these operators are then proxies for stable manifolds. This methodology targets the flow separating nature of manifolds, as illustrated in figure 1.

(vi) *Finite times extended to* $\mathbb{R}$*:* rigorous stable manifolds – in the sense of differential equations theory – can be defined for finite-time systems by artificially extending the time of definition to $\mathbb{R}$ in some way (Sandstede *et al.* 2000; Balasuriya 2012, 2016*b*), enabling comparison with other finite-time methods.

The above list is not exhaustive; there are many other approaches for determining entities which generalise stable manifolds to the finite-time unsteady context (Allshouse & Thiffeault 2012; Balasuriya, Froyland & Santitissadeekorn 2014; Ma & Bollt 2014; Mundel *et al.* 2014; Budišić & Thiffeault 2015; Froyland & Padberg-Gehle 2015; Hadjighasem *et al.* 2016; Oettinger & Haller 2016; Schlueter-Kuck & Dabiri 2017). The large number of methods being developed indicates the difficulties of defining exactly what an analogue of a stable manifold might be in the finite-time situation. (Exponential decay cannot be used as a straightforward criterion in finite time; any time-varying function can be bounded by an expression Ae^{kt} over a finite time interval.) It should also be noted that for $\Lambda(t)$ to be considered a stable manifold proxy over all relevant times, whatever property that is being considered above at time $t^\star$ must be valid for all relevant $t^\star$.

One consideration in thinking of a stable manifold proxy in finite time is whether a stable manifold of a steady flow would be revealed as a stable manifold proxy (using whichever method above) if time were restricted to being finite. Analogously, if $\Lambda(t)$ were a genuine stable manifold for an infinite-time system, would it be recovered if using a finite-time proxy? Fortunately, there are many demonstrations which indicate that under normal conditions, this is indeed so. For example, assorted proxy calculations by Allshouse & Peacock (2015*a*) in the unsteady double gyre (Shadden *et al.* 2005) most often recover the same entities. This gives confidence in the methods in spite of the fact that exact expressions for the stable/unstable manifolds are not available. However, each of the methods is not without its issues (see for example the discussions by Haller (2015) and Balasuriya (2016*a*)); neither are all the methods consistent with each other.

Appendix B. Derivation of control velocity

A formal and very brief derivation of (2.7) is presented here. The legitimacy of this approach relies on the preliminary theoretical work (Balasuriya & Padberg-Gehle 2014*b*) which rigorously establishes that the unsteady control of manifolds is possible via deriving an error bound. The methodology by Balasuriya & Padberg-Gehle (2014*b*) leads to a complicated parametrically defined statement on the control velocity which cannot be implemented easily. In contrast, (2.7) is a direct expression of the control velocity in Eulerian coordinates.

Consider first the case where $\boldsymbol{u}$ is steady. Then, $\tilde{\Gamma}(t) = \Gamma$, which can be represented as a solution to (2.2) such that $\bar{\boldsymbol{x}}(t)$ and where $\bar{\boldsymbol{x}}(t) \to \boldsymbol{a}$ as $t \to \infty$ (if Γ is a stable manifold) or as $t \to -\infty$ (if unstable). Thus, $\bar{\boldsymbol{x}}(p)$ with p as a parameter can identify locations on Γ, as shown in figure 8(*a*). Think of (p, t) as fixed, and τ as variable time. The trajectory $\boldsymbol{x}(t)$ of the controlled system (2.3) on $\Gamma(t)$ at the time t will be at a location $\boldsymbol{x}(\tau)$ on $\Gamma(\tau)$ at time τ, as shown in figure 8(*b*). Its projected point on

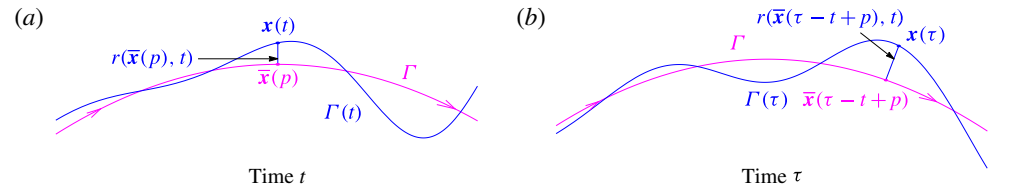

FIGURE 8. (Colour online) Parametrising the manifold for the derivation of the control velocity, with magenta indicating entities associated with the steady uncontrolled system (2.2) and blue the unsteady controlled system (2.3).

the steady manifold Γ is at $\bar{\boldsymbol{x}}(\tau - t + p)$ since the trajectory $\bar{\boldsymbol{x}}$ on Γ following the steady flow (2.2) evolves to this location at time τ. Thus

$$\boldsymbol{x}(\tau) = \bar{\boldsymbol{x}}(\tau - t + p) + r(\bar{\boldsymbol{x}}(\tau - t + p), \tau)\frac{\bar{\boldsymbol{u}}^{\perp}(\bar{\boldsymbol{x}}(\tau - t + p))}{|\bar{\boldsymbol{u}}(\bar{\boldsymbol{x}}(\tau - t + p))|}, \tag{B 1}$$

a crucial way of writing the solution of (2.3) on $\Gamma(\tau)$ which will allow for a surprisingly elementary derivation in terms of Eulerian coordinates. Note that

$$\frac{\mathrm{d}}{\mathrm{d}\tau}[\bar{\boldsymbol{u}}(\bar{\boldsymbol{x}}(\tau - t + p))] = \nabla\bar{\boldsymbol{u}}(\bar{\boldsymbol{x}}(\tau - t + p))\frac{\partial\bar{\boldsymbol{x}}(\tau - t + p)}{\partial\tau} = \nabla\bar{\boldsymbol{u}}(\bar{\boldsymbol{x}}(\tau - t + p))\bar{\boldsymbol{u}}(\bar{\boldsymbol{x}}(\tau - t + p)) \tag{B 2}$$

since $\bar{\boldsymbol{x}}$ is a solution to (2.2), and similarly (details not shown)

$$\frac{\mathrm{d}}{\mathrm{d}\tau}|\bar{\boldsymbol{u}}(\bar{\boldsymbol{x}}(\tau - t + p))| = \frac{\bar{\boldsymbol{u}}^{\top}(\bar{\boldsymbol{x}}(\tau - t + p))\nabla\bar{\boldsymbol{u}}(\bar{\boldsymbol{x}}(\tau - t + p))\bar{\boldsymbol{u}}(\bar{\boldsymbol{x}}(\tau - t + p))}{|\bar{\boldsymbol{u}}(\bar{\boldsymbol{x}}(\tau - t + p))|}, \tag{B 3}$$

where $\bar{\boldsymbol{u}}^{\top}$ is the transpose of $\bar{\boldsymbol{u}}$. Differentiating (B 1) with respect to τ and utilising (B 2), (B 3) and the facts that $\bar{\boldsymbol{x}}$ and $\boldsymbol{x}$ are solutions to (2.2) and (2.3) respectively leads to

$$\bar{\boldsymbol{u}}(\boldsymbol{x}(\tau)) + \boldsymbol{c}(\boldsymbol{x}(\tau), \tau) = \bar{\boldsymbol{u}} + r\left[\frac{|\bar{\boldsymbol{u}}|^2\nabla\bar{\boldsymbol{u}}\bar{\boldsymbol{u}} - \bar{\boldsymbol{u}}(\bar{\boldsymbol{u}}^{\top}\nabla\bar{\boldsymbol{u}}\bar{\boldsymbol{u}})}{|\bar{\boldsymbol{u}}|^3}\right]^{\perp} + \left(\frac{\partial r}{\partial(2)} + \bar{\boldsymbol{u}}\cdot\nabla r\right)\frac{\bar{\boldsymbol{u}}^{\perp}}{|\bar{\boldsymbol{u}}|}, \tag{B 4}$$

where, when not stated, the argument $(\bar{\boldsymbol{x}}(\tau - t + p), \tau)$ is understood, and $\partial r/\partial(2)$ is the derivative with respect to the second (temporal) argument of r. Now, the left-hand side of the above is Taylor expanded using (B 1), and it is assumed that $r = O(\varepsilon)$ and $\boldsymbol{c} = O(\varepsilon)$, where ε is small. Next, higher-order terms in ε are thrown out, and the expression is evaluated at $\tau = t$. This changes the argument $(\bar{\boldsymbol{x}}(\tau - t + p), \tau) \to (\bar{\boldsymbol{x}}(p), t)$, and moreover $\partial r/\partial(2) \to \partial r/\partial t$. With the replacement $\bar{\boldsymbol{x}}(p) \to \boldsymbol{x}$ (i.e. direct Eulerian coordinates on Γ) followed by some algebraic manipulations, the equation

$$\boldsymbol{c} = \left\{\frac{\partial r}{\partial t} + \bar{\boldsymbol{u}}\cdot\nabla r - \frac{\bar{\boldsymbol{u}}\cdot[(\nabla\bar{\boldsymbol{u}})\bar{\boldsymbol{u}}]}{|\bar{\boldsymbol{u}}|^2}r\right\}\frac{\bar{\boldsymbol{u}}^{\perp}}{|\bar{\boldsymbol{u}}|} + \{[(\nabla\bar{\boldsymbol{u}})\bar{\boldsymbol{u}}]^{\perp} - (\nabla\bar{\boldsymbol{u}})\bar{\boldsymbol{u}}^{\perp}\}\frac{r}{|\bar{\boldsymbol{u}}|} \tag{B 5}$$

is obtained. Implicit in this approach is the fact that the specialised solutions on the manifold are moreover attractive. This attraction is in forward time if $\Gamma(t)$ is the unstable manifold (due to the complementary pushing in by the stable manifold near $\boldsymbol{a}$), and in backward time if Γ is stable. Therefore, while the derivation

apparently has not used the specialised property of being on the manifold of the solution $\boldsymbol{x}(t)$, the robustness property of these solutions in the appropriate direction of time automatically ensures that the correct solutions pertaining to the manifolds are obtained. The attracting property is in fact the basis for defining hyperbolic Lagrangian coherent structures for finite-time flow situations (Haller 2015), for which the approach is therefore also valid.

The next issue is to relax the condition that $\boldsymbol{u}$ were steady. If $\boldsymbol{u}$ were time dependent, consider adding the quantity $\bar{\boldsymbol{u}} - \boldsymbol{u}$ to the Eulerian velocity. This would result in a steady flow, with velocity given by $\bar{\boldsymbol{u}}$, for which it is assumed that Γ is a flow barrier. Thus, by adding the quantity $\bar{\boldsymbol{u}} - \boldsymbol{u}$ to (B 5), one gets a full control velocity which when added to $\boldsymbol{u}$ will result in $\Gamma(t)$ as being a flow barrier. This, then, leads to the control expression (2.7).

The control velocity as derived in (2.7) is not the only velocity which engenders $\Gamma(\tau)$ as a manifold. This was derived by moving the trajectory $\bar{\boldsymbol{x}}(\tau)$ (for fixed p) of (2.2) to the trajectory $\boldsymbol{x}(\tau)$ of (2.3) as specified by (B 1). This assumes a specific displacement which is directly in the normal direction to Γ. A curve Γ, however, could be deformed to a given curve $\Gamma(\tau)$ by compressing along Γ first, and then displacing normally. The compression would represent a tangential displacement of each trajectory; this problem was addressed in the inverse direction by Balasuriya (2011) (i.e. given an Eulerian velocity perturbation, what is the resulting deformation of the Lagrangian entity $\Gamma(t)$?). Allowing for such a tangential variation results in much more complicated expressions (Balasuriya 2011), and therefore specifically assuming a purely normal displacement as in (B 1) is a convenient approach. Even with this simplest approach, the final expression (2.7) is not that simple.

Appendix C. Calculations associated with the double-gyre flow

The velocity field (3.4) on $x = 1$ (which shall be called Γ) is

$$\boldsymbol{u}|_{\Gamma} = \begin{pmatrix} \pi A \sin[\pi\delta \sin(\omega t)] \cos(\pi y) \\ -\pi A \cos[\pi\delta \sin(\omega t)] \sin(\pi y) \end{pmatrix}. \tag{C 1}$$

Now, $\boldsymbol{u}$ needs to be time averaged to obtained the steady flow $\bar{\boldsymbol{u}}$ near Γ. The time periodicity of $\boldsymbol{u}$ implies that any suitable interval of width $2\pi/\omega$ can be chosen. Selecting $[-\pi/\omega, \pi/\omega]$, it is clear that $\sin[\pi\delta \sin(\omega t)]$ averages to zero since it is odd, whereas using `Mathematica` (Wolfram Research 2012) gives

$$\frac{\omega}{2\pi} \int_{-\pi/\omega}^{\pi/\omega} \cos[\pi\delta \sin(\omega t)]\, \mathrm{d}t = \mathrm{J}_0(\pi\delta) \quad \Rightarrow \quad \bar{\boldsymbol{u}}(\Gamma) = \begin{pmatrix} 0 \\ -\pi A \mathrm{J}_0(\pi\delta) \sin(\pi y) \end{pmatrix}. \tag{C 2}$$

The invariance of Γ under the steady flow $\boldsymbol{u}$ is obvious from (C 2). Next, $\nabla\bar{\boldsymbol{u}}$ is sought on Γ. Henceforth, superscripts will indicate the component of the vector, whereas subscripts will be the partial derivative. The expression (C 2) gives the fact that, on Γ,

$$\bar{\boldsymbol{u}}^1_y = 0 \quad \text{and} \quad \bar{\boldsymbol{u}}^2_y = -\pi^2 A \mathrm{J}_0(\pi\delta) \cos(\pi y). \tag{C 3a,b}$$

To determine the x-derivative components, consider Taylor-expanding $\boldsymbol{u}$ around $x = 1$ first. Keeping up to leading-order terms in $|x - 1|$ in the first component of (3.4),

$$\boldsymbol{u}^1 = -\pi A \sin[\pi(1 - \varepsilon \sin(\omega t) + (x - 1))] \cos(\pi y). \tag{C 4}$$

Taking the x-derivative and evaluating at $x=1$ yields

$$\boldsymbol{u}^1_x|_\Gamma = \pi^2 A\cos(\pi y)\cos[\pi\delta\sin(\omega t)]. \tag{C 5}$$

When averaged over time, this gives

$$\bar{\boldsymbol{u}}^1_x = \pi^2 A J_0(\pi\delta)\cos(\pi y). \tag{C 6}$$

Keeping only terms to $|x-1|$ in the second component of (3.4) gives

$$\boldsymbol{u}^2 = \pi A\cos[\pi(1-\varepsilon\sin(\omega t)+(x-1))]\sin(\pi y)[2\delta\sin(\omega t)(x-1)+1], \tag{C 7}$$

which when differentiated and evaluated at $x=1$ results in

$$\boldsymbol{u}^2_x|_\Gamma = -2\delta\pi A\sin(\pi y)\sin(\omega t)\cos[\pi\delta\sin(\omega t)]. \tag{C 8}$$

This is an odd function in time, and thus when averaged gives $\bar{\boldsymbol{u}}^2_x = 0$. Applying a Taylor expansion to each of $\bar{\boldsymbol{u}}^{1,2}$ near $x=1$ therefore results in the steady flow (3.7). Moreover, collecting all the derivatives tells us that

$$\nabla\bar{\boldsymbol{u}}(\Gamma) = \begin{pmatrix} \pi^2 A J_0(\pi\delta)\cos(\pi y) & 0 \\ 0 & -\pi^2 A J_0(\pi\delta)\cos(\pi y)\end{pmatrix}. \tag{C 9}$$

The various terms required in (2.7) can now be computed from (C 2) and (C 9). In particular,

$$\frac{\bar{\boldsymbol{u}}^\perp}{|\bar{\boldsymbol{u}}|} = \begin{pmatrix}1\\0\end{pmatrix}, \quad |\bar{\boldsymbol{u}}| = \pi A J_0(\pi\delta)\sin(\pi y) \quad \text{and} \quad \frac{\bar{\boldsymbol{u}}\cdot[(\nabla\bar{\boldsymbol{u}})\bar{\boldsymbol{u}}]}{|\bar{\boldsymbol{u}}|^2} = -\pi^2 A J_0(\pi\delta)\cos(\pi y), \tag{C 10a–c}$$

where it is assumed that $J_0(\pi\delta) > 0$, which occurs when $\delta < 0.76548$. Moreover,

$$[(\nabla\bar{\boldsymbol{u}})\bar{\boldsymbol{u}}]^\perp = \begin{pmatrix} -\pi^3 A^2 J_0(\pi\delta)^2\sin(\pi y)\cos(\pi y)\\ 0\end{pmatrix} \tag{C 11}$$

and

$$(\nabla\bar{\boldsymbol{u}})\bar{\boldsymbol{u}}^\perp = \begin{pmatrix} \pi^3 A^2 J_0(\pi\delta)^2\sin(\pi y)\cos(\pi y)\\ 0\end{pmatrix}. \tag{C 12}$$

Substituting all this information into (2.7) eventually leads to (3.8).

REFERENCES

ALLSHOUSE, M. & PEACOCK, T. 2015*a* Lagrangian based methods for coherent structure detection. *Chaos* **25**, 097617.

ALLSHOUSE, M. & PEACOCK, T. 2015*b* Refining finite-time Lyapunov exponent ridges and the challenges of classifying them. *Chaos* **25**, 087410.

ALLSHOUSE, M. & THIFFEAULT, J.-L. 2012 Detecting coherent structures using braids. *Physica* D **241**, 95–105.

BALASURIYA, S. 2011 A tangential displacement theory for locating perturbed saddles and their manifolds. *SIAM J. Appl. Dyn. Syst.* **10**, 1100–1126.

BALASURIYA, S. 2012 Explicit invariant manifolds and specialised trajectories in a class of unsteady flows. *Phys. Fluids* **24**, 12710.

BALASURIYA, S. 2015 Quantifying transport within a two-cell microdroplet induced by circular and sharp channel bends. *Phys. Fluids* **27**, 052005.

BALASURIYA, S. 2016*a* *Barriers and Transport in Unsteady Flows: a Melnikov Approach*. SIAM.

BALASURIYA, S. 2016*b* Local stable and unstable manifolds and their control in nonautonomous finite-time flows. *J. Nonlinear Sci.* **26**, 895–927.

BALASURIYA, S. 2016*c* Meridional and zonal wavenumber dependence in tracer flux in Rossby waves. *Fluids* **1**, 30.

BALASURIYA, S. & FINN, M. D. 2012 Energy constrained transport maximization across a fluid interface. *Phys. Rev. Lett.* **108**, 244503.

BALASURIYA, S., FROYLAND, G. & SANTITISSADEEKORN, N. 2014 Absolute flux optimising curves of flows on a surface. *J. Math. Anal. Appl.* **409**, 119–139.

BALASURIYA, S., KALAMPATTEL, R. & OUELLETTE, N. 2016 Hyperbolic neighborhoods as organizers of finite-time exponential stretching. *J. Fluid Mech.* **807**, 509–545.

BALASURIYA, S. & PADBERG-GEHLE, K. 2013 Controlling the unsteady analogue of saddle stagnation points. *SIAM J. Appl. Maths* **73**, 1038–1057.

BALASURIYA, S. & PADBERG-GEHLE, K. 2014*a* Accurate control of hyperbolic trajectories in any dimension. *Phys. Rev.* E **90**, 032903.

BALASURIYA, S. & PADBERG-GEHLE, K. 2014*b* Nonautonomous control of stable and unstable manifolds in two-dimensional flows. *Physica* D **276**, 48–60.

BEEBE, D., MOORE, J., BAUER, J., YU, Q., LIU, R., DAVADOSS, C. & JO, B. 2000 Functional hydrogel structures for autonomous flow control inside microfluidic channnels. *Nature* **404**, 588.

BLAZEVSKI, D. & HALLER, G. 2014 Hyperbolic and elliptic transport barriers in three-dimensional unsteady flows. *Physica* D **273**, 46–62.

BOCCALETTI, S., GREBOGI, C., LAI, Y. C., MANCINI, H. & MAZA, D. 2000 The control of chaos: theory and applications. *Phys. Rep.* **329**, 103–197.

BOUJO, E., FANI, A. & GALLAIRE, F. 2015 Second-order sensitivity of parallel shear flows and optimal spanwise-periodic flow modifications. *J. Fluid Mech.* **782**, 491–514.

BOZORGMAGHAM, A., ROSS, S. & SCHMALE, D. 2015 Local finite-time Lyapunov exponent, local sampling and probabilistic source and destination regions. *Nonlinear Process. Geophys.* **22**, 663–677.

BRUNTON, S. & NOACK, B. 2015 Closed-loop turbulence control: progress and challenges. *Appl. Mech. Rev.* **67**, 050801.

BUDIŠIĆ, M., SIEGMUND, S., DOAN, T. & MEZIĆ, I. 2016 Mesochronic classification of trajectories in incompressible 3D vector fields over finite time. *Discrete Continuous Dyn. Syst.* S **9**, 923–958.

BUDIŠIĆ, M. & THIFFEAULT, J.-L. 2015 Finite-time braiding exponents. *J. Nonlinear Sci.* **25**, 087407.

CHEIKH, M. & LAKKIS, I. 2016 Microfluidic transistors for analog microflows amplification and control. *Microfluid Nanofluid* **20**, 91.

COPPEL, W. A. 1978 *Dichotomies in Stability Theory*, Lecture Notes Mathematics, vol. 629. Springer.

CORTELEZZI, L., ADROVER, A. & GIONA, M. 2008 Feasibility, efficiency and transportability of short-horizon optimal mixing protocols. *J. Fluid Mech.* **597**, 199–231.

FISH, F. & LAUDER, G. 2006 Passive and active flow control by swimming fishes and mammals. *Annu. Rev. Fluid Mech.* **38**, 193–224.

FRANCO, E., PEKAREK, D., PENG, J. & DABIRI, J. 2007 Geometry of unsteady fluid transport during fluid structure interactions. *J. Fluid Mech.* **589**, 125–145.

FRANK, P., SCHREITER, J., HAEFNER, S., PASCHEW, G, VOIGT, A. & RICHTER, A. 2016 Integrated microfluidic membrane transistor utilizing chemical information for on-chip flow control. *PLoS ONE* **11**, e0161024.

FROYLAND, G. 2013 An analytical framework for identifying finite-time coherent sets in time-dependent dynamical systems. *Physica* D **250**, 1–19.

FROYLAND, G. & PADBERG, K. 2009 Almost-invariant sets and invariant manifolds – connecting probabilistic and geometric descriptions of coherent structures in flows. *Physica* D **238**, 1507–1523.

FROYLAND, G. & PADBERG-GEHLE, K. 2014 Almost-invariant and finite-time coherent sets: directionality, duration, and diffusion. In *Ergodic Theory, Open Dynamics, and Coherent Structures* (ed. W. Bahsoun, C. Bose & G. Froyland), pp. 171–216. Springer.

FROYLAND, G. & PADBERG-GEHLE, K. 2015 A rough-and-ready cluster-based approach for extracting finite-time coherent sets from sparse and incomplete trajectory data. *Chaos* **25**, 087406.

FROYLAND, G., SANTITISSADEEKORN, N. & MONAHAN, A. 2010 Transport in time-dependent dynamical systems: finite-time coherent sets. *Chaos* **20**, 043116.

GAULTIER, L., DJATH, B., VERRON, J., BRANKART, J. M., BRASSEUR, P. & MELET, A. 2014 Inversion of submesoscale patterns from a high-resolution Solomon sea model: feasibility assessment. *J. Geophys. Res. Oceans* **119**, 4520–4541.

GAULTIER, L., VERRON, J., BRANKART, J.-M., TITAUD, O. & BRASSEUR, P. 2013 On the inversion of submesoscale tracer fields to estimate the surface ocean circulation. *J. Mar. Syst.* **126**, 33–42.

GLASS, O. & HORSIN, T. 2010 Approximate Lagrangian controllability for the 2D Euler quations: application to the control of the shape of a vortex patch. *J. Math. Pures Appl.* **93**, 61–90.

GLASS, O. & HORSIN, T. 2012 Prescribing the motion of a set of particles in a three-dimensional perfect fluid. *SIAM J. Control Optim.* **50**, 2726–2742.

HADJIGHASEM, A., KARRASCH, D., TERAMOTO, H. & HALLER, G. 2016 Spectral clustering approach to Lagrangian vortex detection. *Phys. Rev.* E **93**, 063107.

HALLER, G. 2011 A variational theory of hyperbolic Lagrangian coherent structures. *Physica* D **240**, 574–598.

HALLER, G. 2015 Lagrangian coherent structures. *Annu. Rev. Fluid Mech.* **47**, 137–162.

HALLER, G. & BERON-VERA, F. 2012 Geodesic theory for transport barriers in two-dimensional flows. *Physica* D **241**, 1680–1702.

HALLER, G., HADJIGHASEM, A., FARAZMAND, M. & HIHN, F. 2016 Defining coherent vortices objectively from the vorticity. *J. Fluid Mech.* **795**, 136–173.

HALLER, G. & YUAN, G.-C. 2000 Lagrangian coherent structures and mixing in two-dimensional turbulence. *Physica* D **147**, 352–370.

HASSANZADEH, P., CHINI, G. & DOERING, C. 2014 Wall to wall optimal transport. *J. Fluid Mech.* **751**, 627–662.

HECKMAN, C., SCHWARTZ, I. & HSIEH, M. 2015 Toward efficient navigation in uncertain gyre-like flows. *Intl J. Robot. Res.* **34**, 1590–1603.

HO, C. & TAI, Y. 1998 Micro-electro-mechanical-systems (MEMS) and fluid flows. *Annu. Rev. Fluid Mech.* **30**, 579–612.

IONOV, L., HOUBENOV, N., SIDORENKO, A., STAMM, M. & MINKO, S. 2006 Smart microfluidic channels. *Adv. Funct. Mater.* **16**, 1153–1160.

JADHAV, A., YAN, B., LUO, R., WEI, L., ZHEN, Z., CHEN, C. & SHI, P. 2015 Photoresponsive microvalve for remote actuation and flow control in microfluidic devices. *Biomicrofluidics* **9**, 034114.

JEONG, S.-G., KIM, J., JIN, S., PARK, K. & LEE, C. 2016 Flow control in paper-based microfluidic device for automatic multistep assays: a focused review. *Korean J. Chem. Engng* **33**, 2761–2770.

KARNIK, R., DUAN, C., CASTELINO, K., DAIGUJI, H. & MAJUMDAR, A. 2007 Rectification of ionic current in a nanofluidic device. *Nano Lett.* **7**, 547–551.

KARRASCH, D., FARAZMAND, M. & HALLER, G. 2015 Attraction-based computation of hyperbolic Larangian coherent structures. *J. Comput. Dyn.* **2**, 83–93.

KIM, J. & BEWLEY, T. 2007 A linear systems approach to flow control. *Annu. Rev. Fluid Mech.* **39**, 383–417.

KUCALA, A. & BIRINGEN, S. 2014 Spatial simulation of channel flow instability and control. *J. Fluid Mech.* **738**, 105–123.

LEI, P., ZHANG, J., LI, K. & WEI, D. 2015 Study on the transports in transient flow over impulsively started circular cylinder using Lagrangian coherent structures. *Commun. Nonlinear Sci. Numer. Simul.* **22**, 953–963.

LIN, Z., THIFFEAULT, J.-L. & DOERING, C. R. 2011 Optimal stirring strategies for passive scalar mixing. *J. Fluid Mech.* **675**, 465–476.

MA, T. & BOLLT, E. 2014 Differential geometry perspective of shape coherence and curvature evolution by finite-time nonhyperbolic splitting. *SIAM J. Appl. Dyn. Syst.* **13**, 1106–1136.

MALLORY, K., HSIEH, M., FORGOSTON, E. & SCHWARTZ, I. 2013 Distributed allocation of mobile sensing swarms in gyre flows. *Nonlinear Process. Geophys.* **20**, 657–668.

MANCHO, A. M., WIGGINS, S., CURBELO, J. & MENDOZA, C. 2013 Lagrangian descriptors: a method for revealing phase space structures of general time dependent dynamical systems. *Commun. Nonlinear Sci. Numer. Simul.* **18**, 3530–3557.

MATHEW, G., MEZIĆ, I., GRIVOPOULOS, S., VAIDYA, U. & PETZOLD, L. 2007 Optimal control of mixing in Stokes fluid flow. *J. Fluid Mech.* **580**, 261–281.

MEZIĆ, I., LOIRE, S., FONOBEROV, V. & HOGAN, P. 2010 A new mixing diagnostic and Gulf oil spill movement. *Science* **330**, 486–489.

MICHINI, M., HSIEH, M., FORGOSTON, E. & SCHWARTZ, I. 2014 Robotic tracking of coherent structures in flows. *IEEE Trans. Robot.* **30**, 595–603.

MUNDEL, R., FREDJ, E., GILDOR, H. & ROM-KEDAR, V. 2014 New Lagrangian diagnostics for characterizing fluid flow mixing. *Phys. Fluids* **26**, 126602.

OETTINGER, D. & HALLER, G. 2016 An autonomous dynamical system captures all LCSs in three-dimensional unsteady flows. *Chaos* **26**, 103111.

ONU, K., HUHN, F. & HALLER, G. 2015 LCS tool: a computational platform for Lagrangian coherent structures. *J. Comput. Sci.* **7**, 26–36.

OTT, E., GREBOGI, C. & YORKE, J. A. 1990 Controlling chaos. *Phys. Rev. Lett.* **64**, 1196–1199.

OUELLETTE, N., HOGG, C. & LIAO, Y. 2016 Correlating Lagrangian structures with forcing in two-dimensional flow. *Phys. Fluids* **28**, 015105.

PARK, Y., CHO, K., KANG, J. H., LEE, S. & KIM, J. 2014 Developing a flow control strategy to reduce nutrient load in a reclaimed multi-reservoir system using a 2D hydrodynamic and water quality model. *Sci. Total Environ.* **466–467**, 871–880.

PEACOCK, T. & HALLER, G. 2013 Lagrangian coherent structures: the hidden skeleton of fluid flow. *Phys. Today* **66**, 41–47.

PYRAGAS, K. 1992 Continuous control of chaos by self-controlling feedback. *Phys. Lett.* A **170** (6), 421–428.

RABEN, S., ROSS, S. & VLACHOS, P. 2014 Experimental determination of three dimensional finite time Lyapunov exponents in multi-component flows. *Exp. Fluids* **55**, 1824.

ROM-KEDAR, V., LEONARD, A. & WIGGINS, S. 1990 An analytical study of transport, mixing and chaos in an unsteady vortical flow. *J. Fluid Mech.* **214**, 347–394.

SAMELSON, R. 2013 Lagrangian motion, coherent structures, and lines of persistent material strain. *Annu. Rev. Mar. Sci.* **5**, 137–163.

SANDSTEDE, B., BALASURIYA, S., JONES, C. K. R. T. & MILLER, P. D. 2000 Melnikov theory for finite-time vector fields. *Nonlinearity* **13**, 1357–1377.

SATTARZADEH, S. & FRANSSON, J. 2016 Mastering nonlinear flow dynamics for laminar flow control. *Phys. Rev.* E **94**, 021103.

SCHLUETER-KUCK, K. & DABIRI, J. 2017 Coherent structure coloring: identification of coherent structures from sparse data using graph theory. *J. Fluid Mech.* **811**, 468–486.

SENATORE, C. & ROSS, S. 2008 Fuel-efficient navigation in complex flows. In *Proceedings of 2008 American Control Conference*, pp. 1244–1248; doi:10.1109/ACC.2008.4586663.

SHADDEN, S. 2011 Lagrangian coherent structures. In *Transport and Mixing in Laminar Flows: From Microfluidics to Ocean Currents* (ed. R. Grigoriev), Wiley.

SHADDEN, S. C., LEKIEN, F. & MARSDEN, J. E. 2005 Definition and properties of Lagrangian coherent structures from finite-time Lyapunov exponents in two-dimensional aperiodic flows. *Physica* D **212**, 271–304.

SHARMA, A. & MCKEON, B. 2013 On coherent structure in wall turbulence. *J. Fluid Mech.* **728**, 196–238.

SINHA, S., VAIDYA, U. & RAJARAM, R. 2016 Operator theoretic framework for optimal placement of sensors and actuators for control of nonequilibrium dynamics. *J. Math. Anal. Appl.* **440**, 750–772.

STUART, J. 1967 On finite-amplitude oscillations in laminar mixing layers. *J. Fluid Mech.* **29**, 417–440.

TALLAPRAGADA, P. & ROSS, S. 2013 A set oriented definition of finite-time Lyapunov exponents and coherent sets. *Commun. Nonlinear Sci. Numer. Simul.* **18**, 1106–1126.

TAMASEVICIUTE, E., MAIKOLAITIS, G., BUMELIENE, S. & TAMASEVICIUTE, A. 2013 Stabilizing saddles. *Phys. Rev.* E **88**, 060901(R).

TOUNSI, N., MESTIRI, R., KEIRSBULCK, L., OUALLI, H., HANCHI, S. & ALOUI, F. 2016 Experimental study of flow control on bluff body using piezoelectric actuators. *J. Appl. Fluid. Mech.* **9**, 827–838.

WIGGINS, S. 1992 *Chaotic Transport in Dynamical Systems*. Springer.

WOLFRAM RESEARCH INC. 2012 *Mathematica*, version 9.0 edn. Champaign.